Journal of ELECTRONIC MATERIALS, Vol. 49, No. 5, 2020
https://doi.org/10.1007/s11664-019-07673-x

TOPICAL COLLECTION: INTERNATIONAL CONFERENCE ON THERMOELECTRICS 2019

Enhancing Thermoelectric Properties of Higher Manganese Silicide (HMS) by Partial Ta Substitution

NUTTAWAT PARSE,[1,2] SORA-AT TANUSILP,[3] WANTHANA SILPAWILAWAN,[3] KEN KUROSAKI,[3,4,5] and SUPREE PINITSOONTORN [1,2,6]

1.—Department of Physics, Faculty of Science, Khon Kaen University, Khon Kaen 40002, Thailand. 2.—Institute of Nanomaterials Research and Innovation for Energy (IN-RIE), NANOTEC-KKU RNN on Nanomaterials Research and Innovation for Energy, Khon Kaen University, Khon Kaen 40002, Thailand. 3.—Graduate School of Engineering, Osaka University, 2-1 Yamadaoka, Suita, Osaka 565-0871, Japan. 4.—Research Institute of Nuclear Engineering, University of Fukui, 1-3-33 Kanawa-cho, Tsuruga, Fukui 914-0055, Japan. 5.—Institute for Integrated Radiation and Nuclear Science, Kyoto University, 2, Asashiro-Nishi, Kumatori-cho, Sennan-gun, Osaka 590-0494, Japan. 6.—e-mail: psupree@kku.ac.th

In this work, the thermoelectric properties of the *p*-type higher manganese silicide (HMS) were enhanced by partially substituting Mn with Ta. The ingots of the compound $Mn_{36.4-x}Ta_xSi_{63.6}$, where x = 0.00, 0.25, 0.50. 0.75 and 1.00, were synthesized via arc melting which were then cast into a ribbon shape by a melt spinning process. After that, the crushed ribbons were consolidated to form a bulk sample by spark plasma sintering. The x-ray diffraction analysis showed that the single phase of HMS existed for x up to 0.50. Above that, the evidence of secondary phases was found, confirmed by scanning electron microscope imaging with elemental mapping. For thermoelectric properties measurement, the Seebeck coefficient and electrical conductivity were insignificantly different in the pure-phase samples. On the other hand, the samples with secondary phases showed increased electrical conductivities but slightly decreased Seebeck coefficients. The thermal conductivity was suppressed in all Ta-substituted samples. The lowest lattice thermal conductivity was found in the sample with the impurity phase ($TaSi_2$) due to the enhanced phonon scattering. Consequently, the ZT of the Ta-substituted HMS was enhanced with the peak ZT of 0.37 at 813 K, which is about 28% higher than that of the pristine HMS.

Key words: Thermoelectric, higher manganese silicide, Ta doping, melt spinning, spark plasma sintering

INTRODUCTION

At present, electrical energy has played an important role in daily life due to the increased electricity consumption in smart societies, for example, smartphone, electric car and data mining. Apart from conventional electricity production, there are many alternative resources from which electricity can be harvested, such as solar, wind, water stream, or natural gas from waste. Thermoelectric is an alternative of the candidates for energy harvesting technologies due to many reasons.[1] For instance, it works silently and can harvest energy from various heat sources, especially waste heat produced by machines. Efficiency of thermoelectric devices is defined by the dimensionless figure-of-merit (ZT), expressed by the equation $ZT = S^2\sigma T/\kappa$, where S is the Seebeck coefficient, σ is the electrical

(Received July 15, 2019; accepted September 24, 2019; published online October 3, 2019)

conductivity, κ is the thermal conductivity and T is the absolute temperature.[2] Many thermoelectric materials are being explored for power generation applications, such as germanium telluride,[3] lead telluride,[4,5] half-Heuslers,[6] and silicides.[7–9]

Higher manganese silicide (HMS), one of the thermoelectric silicides, has attracted attention from many research groups and a number of publications have been reported.[10–16] It is a promising p-type TE material due to high oxidation resistance, inexpensive, nontoxic, and abundance on earth.[17,18] HMS has a chemical formula of $MnSi_{\gamma}$ where $\gamma \sim 1.73$ to 1.75. It has a Nowotney chimney ladder (NCL) structure, where a unit cell consists of the tetragonal Mn sublattice based on a β-Sn structure (chimney) and the Si sublattice with the atomic arrangement of coupled helices (ladder).[19,20] There are several compositions of existing HMS phases, such as Mn_4Si_7,[21] $Mn_{11}Si_{19}$,[22] $Mn_{15}Si_{26}$ [23] and $Mn_{27}Si_{47}$.[24] They have the similar lattice parameter a, but different in the lattice parameter c. HMS shows the high thermoelectric performance for the operating temperature range of 400–800°C with the ZT value of $\sim$ 0.4 at 920 K.[25,26] The ZT of HMS can be enhanced through improving synthesis methods, for instance, melt-quenching,[27] wet ball milling,[28] in situ spark plasma sintering (SPS),[29] and Na–Si melt.[30]

In principle, the performance of thermoelectric materials can be improved by reducing the lattice thermal conductivity (κ_l) without altering the electron transport properties.[31–33] Partial substitution of heavy elements in HMS follows such a principle since κ_l is reduced greatly, but the electrical transport is hardly changed.[25] For example, Ghodke et al.[34] reported the synthesis of W-doped HMS via arc melting, melt spinning, and SPS. The presence of W decreased κ_l without altering electron transport properties, leading to the ZT value above 0.5 at 700 K. Furthermore, using the same methods, Yamamoto et al.[25] prepared Re-doped HMS, with maximum ZT around unity, which was attributed to an effective reduction of κ_l but the electron transport was nearly undisturbed. In another work, κ_l approaching minimum limit was found in Re-doped HMS prepared by ball milling and SPS.[26] This indicates the effectiveness of heavy element substitution for suppressing phonon transport. In addition, Chen et al.[27] reported the enhanced thermoelectric power factor ($S^2\sigma$) in Re-doped HMS due to the presence of small islands of MnSi secondary phase.

In this report, we focus on improving the thermoelectric properties of HMS by partial substitution of Ta, a heavy element in the same row as W and Re, for Mn. Ta was reported for the partial substitution in the Al-Mn-Si C40 phase, similar structure to HMS, and the κ was reduced substantially.[35] In this work, $Mn_{36.4-x}Ta_xSi_{63.6}$ intermetallics (x = 0, 0.25, 0.50, 0.75 and 1.0) were fabricated and the thermoelectric properties were investigated and discussed. The Si/Mn ratio was chosen based on the Ref. 25 which is equivalent to $MnSi_{1.747}$. The samples were prepared by arc melting, melt spinning, and followed by SPS. Melt spinning is a well-known rapid solidification process which can enhance the solid solubility of Ta in HMS. Furthermore, SPS is a fast consolidation technique which can minimize the phase segregation.

EXPERIMENTAL PROCEDURES

Si chunk (99.999%), Mn powder (99.9%) and Ta powder (99.99%), purchased from Kojundo Chemical Laboratory Co. Ltd, were used as the starting materials. The samples with the composition of $Mn_{36.4-x}Ta_xSi_{63.6}$ (x = 0, 0.25, 0.50, 0.75 and 1.0) were prepared by weighing Si, Mn and Ta in a stoichiometric ratio. The Mn and Ta powders were compacted into pellets by cold pressing. The pellets and Si chunk were melted and re-melted several times by arc melting (AM) under pressurized argon atmosphere. The obtained ingots were crushed and loaded in the melt spinning (MS) machine. The ingot ($\sim$ 1.3 g) was re-melted in a boron nitride nozzle (0.6 mm diameters) and injected onto a copper wheel (20 cm diameters) rotating at 4500 rpm. The process was done in an argon atmosphere. The melt spun ribbons were ground into powders by using a mortar and a pestle. The powders were sintered in a graphite die (12.7 mm diameters) by spark plasma sintering (SPS) at 1123 K and 60 MPa under vacuum atmosphere and holding time of 5 min.

The microstructure of the samples was observed by the x-ray diffraction analysis (XRD, Ultima IV, Rigaku) and scanning electron microscopy (SEM, JSM-6500F, JEOL). For thermoelectric measurement, thermal conductivity was calculated by $\kappa = \alpha C_p \rho$, where α, C_p, ρ are thermal diffusivity, heat capacity, and density, respectively. The α was measured by using a flash diffusivity apparatus (Netzsch LFA-457) from room temperature to 1073 K under Ar atmosphere. The C_p was calculated from $3nR$, (n and R are the numbers of atoms per formula unit and the gas constant). The ρ was measured from the weight and dimensions of the samples. Seebeck coefficient (S) and electrical conductivity (σ) were measured by the commercial thermoelectric measurement apparatus (ULVAC ZEM-3) from room temperature to 1073 K under He atmosphere. Hall coefficient was measured by the Van der Pauw technique with a Hall measurement system (Tokyo Resitest8300) at room temperature under an applied magnetic field of 0.5 T.

RESULTS AND DISCUSSION

XRD analysis was performed for all samples after AM, MS, and SPS. As shown in Figure S1 (Supplementary Information), the XRD patterns of the ground AM ingots show that apart from the majority phase of HMS, the impurity phases such as Si,

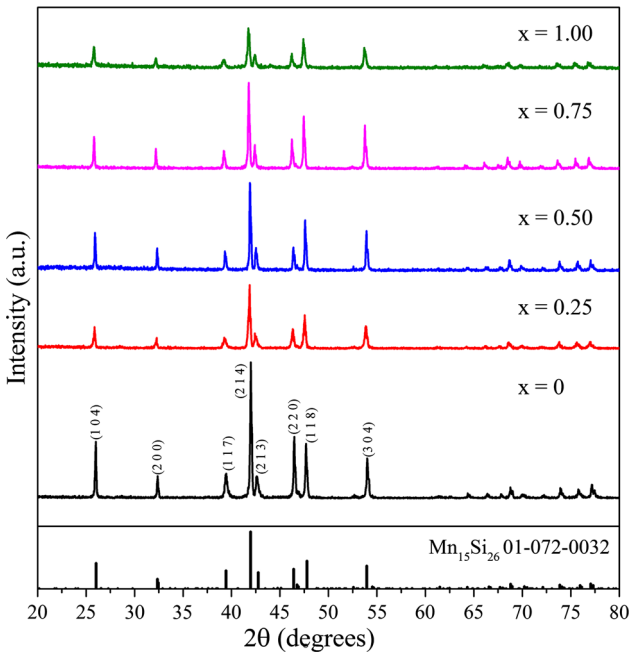

Fig. 1. XRD patterns of the $Mn_{36.4-x}Ta_xSi_{63.6}$ ribbon samples from the melt spinning (MS) process.

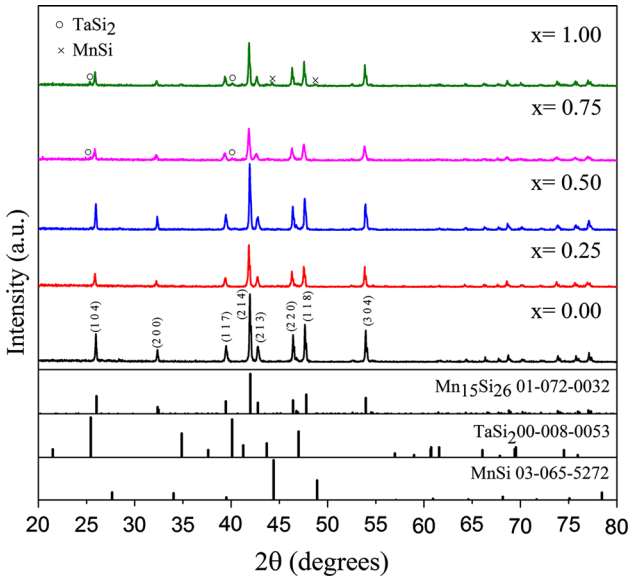

Fig. 2. XRD patterns of the $Mn_{36.4-x}Ta_xSi_{63.6}$ bulk samples after SPS.

MnSi, and $TaSi_2$ are observed for all samples. After MS, the XRD patterns of the crushed ribbons are shown in Fig. 1. The single phase of HMS without any visible secondary phase is found. It indicates the advantage of the MS technique in fabricating single phase intermetallic compounds due to the rapid solidification of the melt spun ribbon.[36,37] The SPS samples were crushed and ground before XRD analysis and the XRD patterns are shown in Fig. 2. The pure HMS phase was observed in the Ta-substituted samples for x up to 0.5, whereas the impurity phases ($TaSi_2$ and MnSi) were observed for x above 0.5. The presence of the impurity phases after SPS is attributed to the high temperature process of SPS that drives the segregation of thermodynamically stable phases. The lattice constants of the HMS phase were calculated as shown in Table I. The lattice constants (both a and c) increased with increasing Ta concentration up to $x = 0.5$. Thus, it is inferred that the solubility of Ta in the $Mn_{36.4-x}Ta_xSi_{63.6}$ compounds is limited to 0.5 at.%. It would be useful to compare the results with the solubility limit of Ta in the HMS in the thermodynamically equilibrium state. Unfortunately, the phase diagram for HMS and Ta, as well as the ternary phase diagram of Mn–Si-Ta, cannot be found anywhere. Table I also presents the density and relative density, which shows the values above 90% for all samples. The dense samples are important for good thermoelectric properties.

Since the XRD results show the single HMS for the sample with $x = 0$, 0.25 and 0.5, and the existence of second phases above that, it is worth to do further analysis using SEM for the sample with x below and above 0.5, as illustrated in Figs. 3 and 4. Figure 3 shows the SEM image along with the energy dispersive x-ray spectroscopy (EDX) mapping images of the sample with $x = 0.25$. The surface morphology in Fig. 3a shows that the sample is very dense but some surface defects can be observed probably due to the sample preparation, such as cutting, grinding or polishing. However, the precipitation of second phases is not seen in the SEM image. It is confirmed from the EDX mapping images (Fig. 3b, c and d) which have the homogeneous distribution of all elements (Mn, Si, Ta). On the other hand, the SEM image with the corresponding EDX maps of the sample with $x = 0.75$ is presented in Fig. 4. The SEM image (Fig. 4a) shows the obvious segregation of the second phase as the bright clusters of particles. In the same area, the EDX images show the Mn-depleted region and the Si- and Ta- enriched region. Thus, the presented second phases are likely to be $TaSi_2$ phase, agreeing with the XRD analysis. The existence of the impurity phases has a significant effect on thermoelectric properties as described shortly.

The temperature dependent electron transport properties of the bulk $Mn_{36.4-x}Ta_xSi_{63.6}$ intermetallic compounds ($x = 0$, 0.25, 0.50, 0.75 and 1.0) are shown in Fig. 5, (with the power factor in Figure S2, Supplementary Information). The Seebeck coefficients (S) of all samples increase with temperature to about 770 K and then decrease with temperature (Fig. 5a). The positive values of S indicate p-type conduction, consistent with the Hall measurement (Table I). It is obvious that the S values can be divided into two groups. The first group consists of the samples with $x = 0$, 0.25, 0.50, which are associated with the HMS single phase from the XRD analysis. In the second group (for $x = 0.75$ and 1.0), the second phases ($TaSi_2$ and MnSi) are presented. $TaSi_2$ exhibited a metallic nature with

Table I. Nominal composition, lattice constant, density, carrier concentration (n) and mobility (μ) at 300 K for the $Mn_{36.4-x}Ta_xSi_{63.6}$ samples

Nominal composition	a (Å)	c (Å)	Density (g/cm^3)	Relative density (%)	n (10^{20} cm^{-3})	μ (cm^2 V^{-1} s^{-1})
x = 0	5.530	65.511	4.96	96	11.4	2.6
x = 0.25	5.546	65.610	4.76	92	4.53	7.3
x = 0.50	5.549	65.671	4.91	95	2.36	10.3
x = 0.75	5.545	65.674	5.01	97	2.30	39.6
x = 1.00	5.541	65.625	5.11	99	2.24	54.8

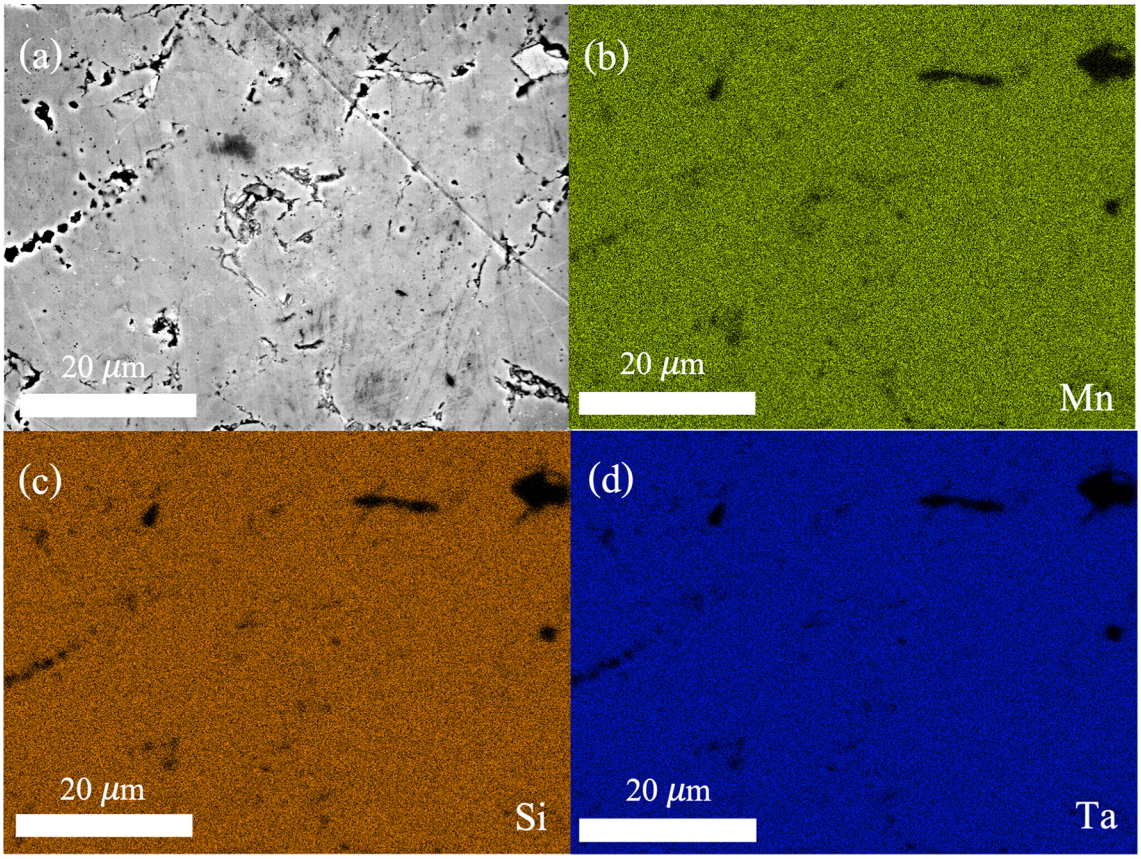

Fig. 3. The SEM image (a) with the corresponding EDX mapping (b–d) of the Ta-doped HMS sample for x = 0.25.

a very large conductivity.[38,39] Also, the presence of MnSi phase in HMS was reported to deteriorate thermoelectric properties.[28] Hence, the formation of the second phases likely contributed to the drop in the S values. This interpretation is supported by the electrical conductivity (σ) measurement, as shown in Fig. 5b. The σ values for the single phase HMS samples (x = 0–0.5) are relatively lower than the samples containing the second phases (x = 0.75, 1.00). The presence of the intermetallic second phases contributed to large conduction of charge carrier. In addition, below 770 K, σ decreases with increasing temperature, indicating the metallic conducting behavior, whereas above 770 K, σ increases with temperature implying semiconducting behavior. This observation is consistent with the previous studies of HMS.[29,30,40]

Amongst the samples with single HMS phase (x = 0–0.5), the values of S and σ are not significantly different. Generally, S can be determined by the Mott formula expressed as:[41]

$$S = \frac{c_e}{n} + \frac{\pi^2 k_B^2 T}{3e}\left[\frac{\partial \ln \mu(\varepsilon)}{\partial \varepsilon}\right]_{\varepsilon=\varepsilon_F}, \quad (1)$$

where c_e, n, k_B, e, $\mu(\varepsilon)$ are electronic specific heat, carrier concentration, Boltzmann constant, elementary charge, and energy correlated carrier mobility, respectively. The Hall measurement at room temperature for the carrier concentration (n) and mobility (μ) is shown in Table I. From Eq. 1, if the first term dominates, S is inversely proportional to n. However, this is not the circumstance for our case since n decreased with Ta substitution (Table I) but

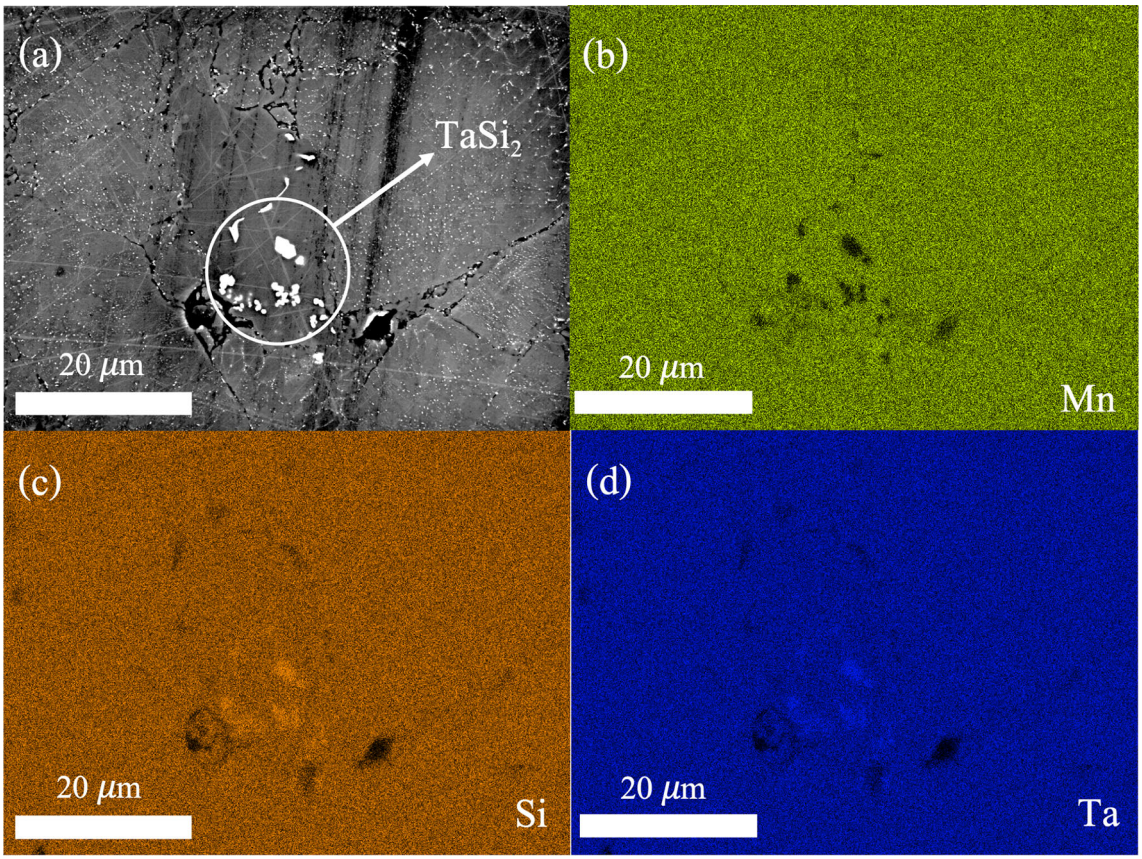

Fig. 4. The SEM image (a) with the corresponding EDX mapping (b–d) of the Ta-doped HMS sample for $x = 0.75$.

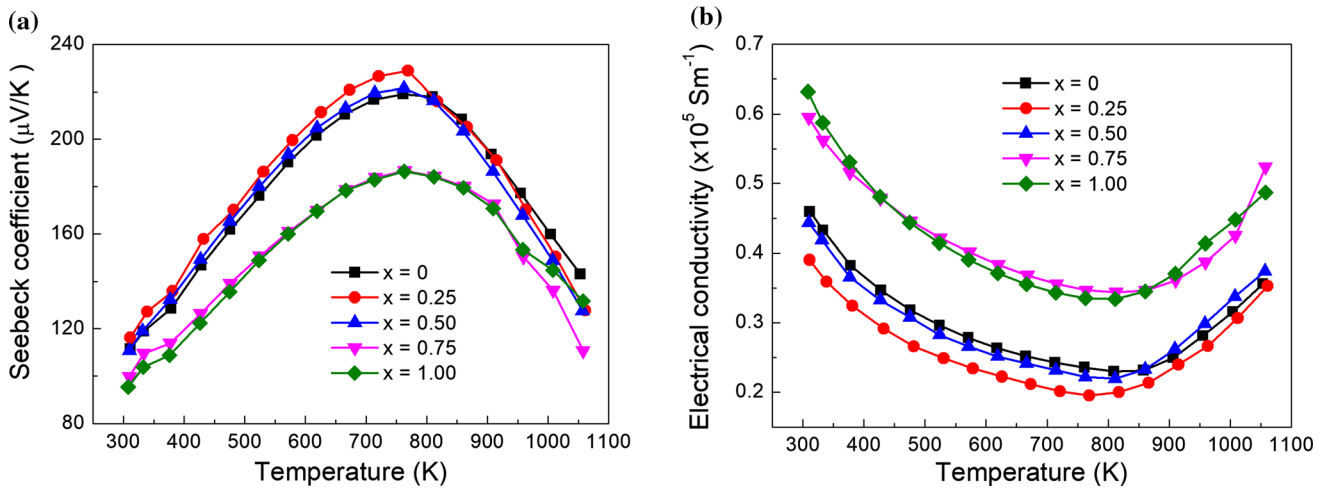

Fig. 5. Temperature dependent electrical transport properties of the $Mn_{36.4-x}Ta_xSi_{63.6}$ samples: (a) Seebeck coefficient and (b) electrical conductivity.

S is relatively independent. It is inferred that the second term in Eq. 1 must be dominant. The second term in Eq. 1 is closely related to the electronic band structure of HMS,[42] and the partial substitution of Ta may not cause the change of the band near Fermi level. This interpretation is justified since a very small amount of Ta was substituted for Mn. On the other hand, the invariance of σ for the sample with $x = 0$–0.5 can be explained by considering both n and μ as presented in Table 1. The electrical conduction of a single-type charge carrier can be determined from $\sigma = ne\mu$, where e is the charge of the electron.[43,44] Since n increases with x but μ decreases with x, it is, hence, understandable that the σ values do not change in Ta concentration.

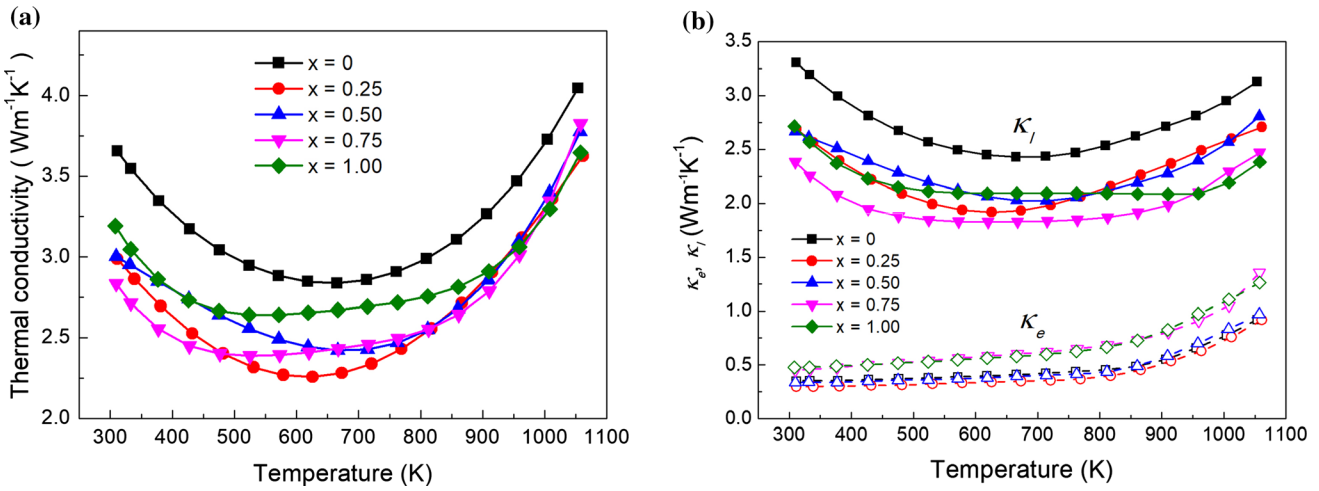

Fig. 6. Temperature dependent thermal conductivity of the $Mn_{36.4-x}Ta_xSi_{63.6}$ samples: (a) total thermal conductivity and (b) lattice and electronic thermal conductivity.

Thermal conductivities (κ) of the Ta-doped HMS samples are shown in Fig. 6a. In every sample, κ initially decreases with increasing temperature from phonon–phonon scattering contribution. At higher temperature (above 600–700 K), κ increases with temperature which could be due to the effect of bipolar conduction.[45] All Ta-doped samples show the decreased κ for the whole temperature range. Noticeably, the lowest κ belongs to the sample with $x = 0.25$ attributed to the lowest density of this sample. The total thermal conductivity (κ) is contributed from two components: the lattice thermal conductivity (κ_l) and the electronic thermal conductivity (κ_e): $\kappa = \kappa_l + \kappa_e$. The electronic thermal conductivity can be estimated from the Wiedemann–Franz law[46] $\kappa_e = L\sigma T$, where L is the Lorenz number, approximately 2.44×10^{-8} W Ω K^{-2} for a degenerate semiconductor. Therefore, κ_l and κ_e can be calculated and are represented in Fig. 6b. It is obviously seen that κ_l was suppressed in the doped sample compared to the undoped HMS due to the presence of Ta atoms which increase lattice distortion and point defect scattering.[47,48] The sample with the lowest κ_l is for $x = 0.75$. In addition to the lattice distortion and point defect scattering by Ta doping, this sample possesses impurity phase ($TaSi_2$) on a micrometer scale. The presence of the impurity phase also contributes to the phonon scattering, and thus further suppressed κ_l. However, it is difficult to estimate the reduction of κ_l due to the presence of micro $TaSi_2$ precipitate from theoretical point of view. On the other hand, κ_e tends to increase with temperature which could be due to bipolar effect.[45,49] The samples with impurity phases ($x = 0.75$ and 1.00) show larger κ_e since the presence of intermetallic phases could contribute to larger electronic thermal conduction.[38,50,51]

Finally, the ZT of the bulk $Mn_{36.4-x}Ta_xSi_{63.6}$ samples is displayed in Fig. 7. The ZT increases with temperature to the maximum point around

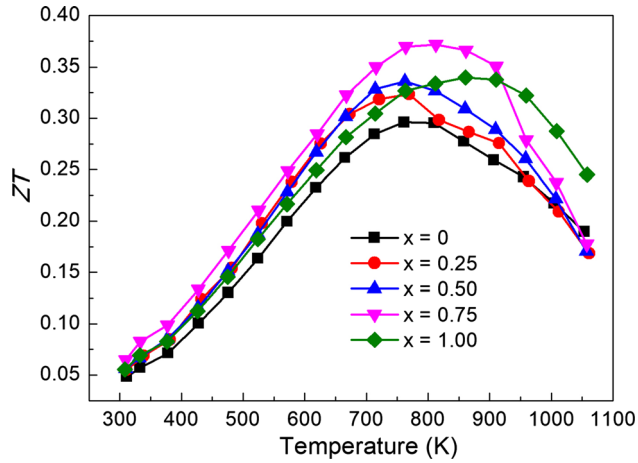

Fig. 7. Temperature dependent ZT of the $Mn_{36.4-x}Ta_xSi_{63.6}$ samples.

750–800 K before decreasing. The peak ZT of the pristine HMS is 0.29 at 761 K. For the Ta-doped HMS sample, the highest ZT is for the sample with $x = 0.75$, with the peak ZT of 0.37 at 813 K, about a 28% increase compared to the pristine HMS. Although this sample contains the $TaSi_2$ impurity phase, it was proved to be advantageous in several aspects. The impurity phase contributes to larger σ due to its intermetallic nature with higher electrical conduction. Moreover, the presence of impurity inclusions enhances phonon scattering, leading to low κ_l. However, the ZT in the present work is relatively still low probably due to the low solubility limit of Ta in HMS as compared to another elemental substitution, e.g., Re [16,26,27] and W.[34,35] Further improvement of the ZT in Ta-doped HMS could be possible via other synthesis methods to enhance the solubility limit, or the utilization of secondary phases and their distribution.

CONCLUSION

We have synthesized Ta-doped HMS bulk sample ($Mn_{36.4-x}Ta_xSi_{63.6}$) by AM, subsequent MS, and densified by SPS. The bulk samples show a high density of more than 90% of the theoretical values. The crystallinity and solubility limit of Ta in HMS was determined by XRD analysis. It was found that for $x = 0$, 0.25, 0.50, the single phase of HMS was obtained whereas for $x = 0.75$ and 1.00, the presence of the secondary phases was found as confirmed by SEM imaging and EDX mapping. The presence of the secondary phase ($TaSi_2$) in the sample with $x = 0.75$ was found to be advantageous since it contributes to higher electron conduction as well as stronger phonon scattering. As a result, the σ and κ_l was the lowest for the sample with $x = 0.75$. This led to the highest ZT with the peak value of 0.37 at 813 K, 28% larger with respect to the Ta-free HMS sample.

ACKNOWLEDGMENTS

This work was supported by the Thailand Research Fund (TRF) in cooperation with Synchrotron Light Research Institute (public organization) and Khon Kaen University (RSA6280020), the Research Network NANOTEC (RNN) program of the National Nanotechnology Center (NANOTEC), NSTDA, Ministry of Higher Education, Science, Research and Innovation and Khon Kaen University, the National Research Council of Thailand through Khon Kaen University (6200071). N.P. would like to thank the scholarship from the Development and Promotion of Science and Technology program, Thailand.

ELECTRONIC SUPPLEMENTARY MATERIAL

The online version of this article (https://doi.org/10.1007/s11664-019-07673-x) contains supplementary material, which is available to authorized users.

REFERENCES

1. B.I. Isamail and W.H. Ahmed, *Recent Patents Electr. Eng.* 2, 27–39 (2009).
2. D.M. Rowe, *CRC Handbook of Thermoelectrics* (Boca Raton, CRC Press, 1995).
3. E. Hazan, N. Madar, M. Parag, V. Casian, O. Ben-Yehuda, and Y. Gelbstein, *Adv. Electron. Mater.* 1, 1500228 (2015).
4. I. Cohen, M. Kaller, G. Komisarchik, D. Fuks, and Y. Gelbstein, *J. Mater. Chem. C* 3, 9559–9564 (2015).
5. G.M. Guttmann, D. Dadon, and Y. Gelbstein, *J. Appl. Phys.* 118, 065102 (2015).
6. O. Appel and Y. Gelbstein, *J. Electron. Mater.* 43, 1976–1982 (2014).
7. Y. Sadia, Z. Aminov, D. Mogilyansky, and Y. Gelbstein, *Intermetallics* 68, 71–77 (2016).
8. K. Kurosaki, A. Yusufu, Y. Miyazaki, Y. Ohishi, H. Muta, and S. Yamanaka, *Mater. Trans.* 57, 1018–1020 (2016).
9. W. Liu, K. Yin, Q. Zhang, C. Uher, and X. Tang, *Natl. Sci. Rev.* 4, 611–626 (2017).
10. A.J. Zhou, X.B. Zhao, T.J. Zhu, Y.Q. Cao, C. Stiewe, R. Hassdorf, and E.J. Muller, *J. Electron. Mater.* 38, 1072–1077 (2009).
11. W. Luo, H. Li, Y. Yan, Z. Lin, X. Tang, Q. Zhang, and C. Uher, *Intermetallics* 19, 404–408 (2011).
12. A. Famengo, S. Battiston, M. Saleemi, S. Boldrini, S. Fiameni, F. Agresti, and M.S. Toprak, *J. Electron. Mater.* 42, 2020–2024 (2013).
13. Y. Sadia, N. Madar, I. Kaler, and Y. Gelbstein, *J. Electron. Mater.* 44, 1637–1643 (2014).
14. S.N. Girard, X. Chen, F. Meng, A. Pokhrel, J. Zhou, L. Shi, and S. Jin, *Chem. Mater.* 26, 5097–5104 (2014).
15. Z. Gao, Z. Xiong, J. Li, C. Lu, G. Zhang, T. Zeng, Y. Ma, R. Zhang, K. Chen, T. Zhang, Y. Liu, J. Yang, L. Cao, and K. Jin, *J. Mater. Chem. A* 7, 3384 (2019).
16. T. Homma, T. Kamata, N. Saito, S. Ghodke, and T. Takeuchi, *J. Alloys Compd.* 776, 8–15 (2019).
17. D.K. Shin, S.W. You, and I.H. Kim, *J. Korean Phys. Soc.* 65, 1499–1502 (2014).
18. M.I. Fedorv, V.K. Zaitsev, F.Y. Solomkin, and M.V. Vendernikov, *Tech. Phys. Lett.* 23, 602–603 (1997).
19. Y. Miyazaki, D. Igarashi, K. Hayashi, T. Kajitani, and K. Yubuta, *Phys. Rev. B* 78, 214104 (2008).
20. J.M. Higgins, A.L. Schmitt, I.A. Guzei, and S. Jin, *J. Am. Chem. Soc.* 130, 16086–16094 (2008).
21. U. Gottlieb, A. Sulpice, B. Lambert-Andron, and O.J. Lavorde, *J. Alloys Compd.* 361, 13–18 (2003).
22. O. Shwomma, A. Preisinger, H. Nowotny, and A. Wittman, *Monatsh. Chem.* 95, 1527–1537 (1969).
23. G. Zwilling and H. Nowotny, *Monatsh. Chem.* 102, 672–677 (1971).
24. G. Zwilling and H. Nowotny, *Monatsh. Chem.* 104, 668–675 (1973).
25. A. Yamamoto, S. Ghodke, H. Miyazaki, M. Inukai, Y. Nishino, M. Matsunami, and T. Takeuchi, *Jpn. J. Appl. Phys.* 55, 020301 (2016).
26. X. Chen, S.N. Girard, F. Meng, E. Lara-Curzio, S. Jin, B. Goodeough, J. Zhou, and L. Shi, *Adv. Energy Mater.* 4, 1400452 (2014).
27. X. Chen, J. Zhou, B.J. Goodenough, and L. Shi, *J. Mater. Chem. C* 3, 10500–10508 (2015).
28. D.N. Truong, H. Kleinke, and F. Gascoin, *Intermetallics* 66, 127–132 (2015).
29. G. Liu, Q. Lu, X. Zhang, J. Zhang, and Y. Shi, *J. Electron. Mater.* 41, 1450–1455 (2012).
30. T. Yamada, Y. Miyazaki, and H. Yamane, *Thin Solid Films* 519, 8524–8527 (2011).
31. B.C. Sales, *MRS Bull.* 23, 15–21 (1998).
32. G.J. Snyder, M. Christensen, E. Nishibori, T. Caillat, and B.B. Iversen, *Nat. Mater.* 3, 458–463 (2004).
33. K. Biswas, J. He, I.D. Blum, C.I. Wu, T.P. Hogan, D.N. Seidman, and M.G. Kanatzidis, *Nature* 489, 414–418 (2012).
34. S. Ghodke, N. Hiroishi, A. Yamamoto, H. Ikuta, M. Matsunami, and T. Takeuchi, *J. Electron. Mater.* 45, 5279–5284 (2016).
35. A. Yamamoto, H. Miyazaki, M. Inukai, Y. Nishino, and T. Takeuchi, *Jpn. J. Appl. Phys.* 54, 071801 (2015).
36. G. Tan, Y. Zheng, and X. Tang, *Appl. Phys. Lett.* 103, 183904 (2013).
37. G. Tan, W. Liu, S. Wang, Y. Yan, H. Li, X. Tang, and C. Uher, *J. Mater. Chem. A* 1, 12657 (2013).
38. H.-C. Cho, S.-H. Paek, J.-S. Choi, and Y.-S. Hwang, *Thin Solid Films* 221, 203–206 (1992).
39. L. Jin, Master thesis. The New Jersey Institute of Technology, New Jersey, USA (2011).
40. Z. Zammanipour, X. Shi, M. Mozafari, J.S. Krasinski, L. Tayebi, and D. Vashaee, *Ceram. Int.* 39, 2353–2358 (2013).
41. Y. Wang, Y. Sui, P. Ren, L. Wang, X. Wang, W. Su, and H. Fan, *Chem. Mater.* 22, 1155–1163 (2010).

42. D.B. Migas, V.L. Shaposhnikov, A.B. Filonov, V.E. Borisenko, and N.N. Dorozhkin, *Phys. Rev. B* 77, 075205 (2008).
43. X. Zhang and L.-D. Zhao, *J. Materiomics* 1, 92–105 (2015).
44. G.J. Snyder and E.S. Toberer, *Nat. Mater.* 7, 105–114 (2008).
45. J. Bahk and A. Shakouri, *Appl. Phys. Lett.* 105, 052106 (2014).
46. E. Maciá-Barber, *Thermoelectric Materials: Advances and Applications* (Singapore, Pan Stanford Publishing, 2015).
47. Y. Nishino and S. Deguchi, *Phys. Rev. B* 74, 115115 (2006).
48. Y. Nishino and I.O.P. Conf, *Ser. Mater. Sci. Eng.* 18, 142001 (2011).
49. S. Wang, J. Yang, T. Toll, J. Yang, W. Zhang, and X. Tang, *Sci. Rep.* 5, 10136 (2015).
50. S.P. Murarka and D.B. Fraser, *J. Appl. Phys.* 51, 1593–1598 (1980).
51. A.E. Petrova, E.D. Bauer, V. Krasnorussky, and S.M. Stishov, *Phys. Rev. B* 74, 092401 (2006).